Nano Research
2021, 14(3): 635–645

ISSN 1998-0124 CN 11-5974/O4
https://doi.org/10.1007/s12274-020-3084-2

Research Article

Flexible synthesis of high-purity plasmonic assemblies

Laurent Lermusiaux[†], Anum Nisar, and Alison M. Funston (✉)

ARC Centre of Excellence in Exciton Science and School of Chemistry, Monash University, Clayton, VIC 3800, Australia
[†] Present address: Université de Bordeaux, CNRS, ICMCB, UMR 5026, Pessac 33600, France

© Tsinghua University Press and Springer-Verlag GmbH Germany, part of Springer Nature 2020
Received: 13 May 2020 / **Revised:** 1 September 2020 / **Accepted:** 2 September 2020

ABSTRACT

The self-assembly of nanoparticles has attracted a vast amount of attention due to the ability of the nanostructure to control light at the sub-wavelength scale, along with consequent strong electromagnetic field enhancement. However, most approaches developed for the formation of discrete assemblies are limited to a single and homogeneous system, and incorporation of larger or asymmetrical nanoparticles into assemblies with high purity remains a key challenge. Here, a simple and versatile approach to assemble nanoparticles of different sizes, shapes, and materials into various discrete homo- or hetero-structures using only two complementary deoxyribonucleic acid (DNA) strands is presented. First, surface functionalisation using DNA and alkyl-polyethylene glycol (PEG) enables transformation of as-synthesised nanoparticles into readily usable plasmonic building blocks for self-assembly. Optimisation of the DNA coverage enables the production of different assembly types, such as homo- and hetero-dimers, trimers and tetramers and core-satellite structures, which are produced in high purity using electrophoresis purification. The approach is extended from purely plasmonic structures to incorporate (luminescent) semiconductor nanoparticles for formation of hybrid assemblies. The deposited assemblies form a high yield of specific geometrical arrangements, attributed to the van der Waals attraction between particles. This method will enable the development of new complex colloidal nanoassemblies for biological and optical applications.

KEYWORDS

deoxyribonucleic acid (DNA) self-assembly, electrophoretic purification, nanoparticle assemblies, colloidal stability

1 Introduction

A key challenge in nanoscience is the precise arrangement of individual nanocrystals, of different materials, into specific assemblies on the nanoscale [1–3]. This challenge becomes even more demanding for asymmetric nanoparticles [4]. The successful implementation of methods to achieve this promises to open pathways for the formation of functional nanoscale superstructures. Over the past decade developments in colloidal chemistry have allowed the synthesis of nanocrystals of different materials, shapes and sizes. With these as building blocks, the potential number of combinations in material, nanocrystal spatial arrangement and geometry is immense. The assembly of metallic nanoparticles into discrete superstructures is motivated by the possibility of controlling electromagnetic fields at the nanoscale via coupling of the nanoparticle plasmon resonances. The resultant electromagnetic enhancement (in the near-field) and interparticle separation dependant spectral response have been exploited for surface-enhanced Raman spectroscopy [5], fluorescence enhancement [6], chemical sensors [7], and the development of therapeutic and imaging agents [8, 9].

Due to the vast number of different ways of assembling particles, many assembly geometries can be potentially achieved, including homo-, hetero- dimers/trimers/tetramers along with core–satellite assemblies and Janus structures [10]. Significant progress towards achieving general schemes for assembly of discrete assemblies with the flexibility to incorporate different materials, shapes, and sizes has been made [11]; however, the majority of self-assembled structures reported remain gold homostructures. Even then, the controlled assembly of particles into discrete structures has been achieved mostly for spherical nanocrystals [6, 12–20], with a few reports of assembly of homodimers of nanotriangles [21], nanocubes [22], and bipyramids with limited yields [23].

Incorporation of different particles (shape/size/material) into one assembly with a translatable technique is a key requirement for the facile synthesis of functional nanoassemblies. Heterostructures exhibit a broad range of optical properties [24–31], with numerous potential applications including photocatalysts [32] and plasmon-induced transparency [33]. However, formation of these within a general assembly scheme is a complex process due to the different combinations of solvents, reactants, and surfactants necessary to synthesise different particles. These confer drastically different physico-chemical surface properties; for example, gold nanoparticles compared to semiconductor nanoparticles such as CdSe. Therefore, it is more complicated to achieve the same surface properties across different nanoparticles and control the fine balance between attractive and repulsive forces required to form a stable structure. Consequently, assembly schemes developed to produce homostructures cannot necessarily be translated to other nanoparticles in a straightforward manner.

The fabrication of nanocrystal superstructures is governed by the choice of the linker, physical, or chemical, between the nanocrystals as this greatly influences the interparticle distances, the structural flexibility, and the positioning of the different particles [25]. Self-assembly has been achieved using electrostatic

Address correspondence to alison.funston@monash.edu

interactions between oppositely charged nanoparticles [24, 27, 34] or a chemical linker attached to different particles utilising coordination chemistry [35], Ag soldering [36], polymeric glue [28], dithiol linkers [37], dihydroxy-citrate interactions [38], capillary-assisted particle assembly over topographical templates [29, 39], protein [40], and deoxyribonucleic acid (DNA). Among these approaches, DNA is a highly versatile tool to produce controlled assemblies thanks to the specific recognition of complementary nucleobases [16]. Engineering DNA sequences enables control of the distance between the particles. Nanoparticle self-assembly using DNA can be direct, i.e. complementary strands are attached to particles, or templated, i.e. particles attach onto a DNA template, usually an origami DNA [41]. The former, more economical in terms of DNA strands, usually yields structures with small interparticle distances but little control over the particle positioning [42]. The latter can be used to precisely position nanoparticles and form large nanoassemblies as the overall size is imposed by the long DNA scaffold [30–31, 43–46]. However, the high ionic strength required to stabilise the compact DNA origami makes it challenging to assemble less colloidally stable nanoparticles. Moreover, the high cost of redesigning the numerous staple strands to customise origamis for a given set of particles makes this approach not yet fully versatile and accessible. It is clear that the development of an assembly method suitable for application across a vast library of nanoparticles would allow the synthesis of new and unique superstructures with high purity and high structural uniformity.

Directed DNA self-assembly of nanoparticles in solution is driven by the DNA coverage onto the different building blocks. Low DNA coverage produces discrete structures [17] whereas high coverage promotes formation of micron-size crystals [47, 48]. Isolating nanoparticles with controlled DNA valency is possible from solutions of nanoparticles with low DNA coverage (where the number of strands attached follow a Poisson distribution [49]) using electrophoresis. This approach is used to produce discrete structures of a given geometry and/or number of particles in high yield [19, 50–54] but is mostly limited to small particles (usually around 10 nm) [55, 56]. For larger particles, the size increase due to the addition of the linker molecule onto the nanoparticle surface is very small (compared to the bare particles). Therefore sufficient separation of particles with only one linker using volume/charge based methods is not achieved [57]. Anisotropic nanoparticles are generally larger than the small gold spheres (~ 10 nm) for which this separation has been reported. Anisotropic nanocrystals also bring the additional complexity of controlling the nanocrystal orientations within the assembly (with respect to one another). As the optical properties of the structures are intrinsically related to the arrangement of the anisotropic building blocks [21, 58], in order to achieve samples with uniform optical properties and surface-enhanced Raman scattering (SERS) responses, reproducible placement is imperative. Achieving then, discrete assemblies of larger and/or asymmetric nanoparticles with high purity for any given dimer with only one morphology has remained largely elusive.

In this paper we describe a versatile and simple self-assembly approach that produces different plasmonic assemblies of high purity. The method is applicable across many as-synthesised nanoparticles of different sizes, shapes and materials (metallic or semiconductor) and uses just two complementary DNA strands. This approach is based on the passivation of particles of various surface chemistry with a thiol-alkyl-polyethylene glycol (PEG), instead of the more common thiol-PEG, making them colloidally very stable, negatively charged and readily suitable for electrophoresis. We explain how to control the DNA valency of the nanoparticles to favour the production and purification of different types of assembly: homo- and hetero-structures and core–satellites. Upon deposition on a substrate, assemblies tend to maximise the surface contact between the nanoparticles producing high yields of specific orientation with small interparticle distances.

2 Results and discussion

2.1 General assembly scheme

The self-assembly scheme to produce various types of plasmonic assemblies in high purity is derived from classical DNA-directed approaches and is outlined in Scheme 1. We define "purity" here as the yield of the desired structure type, compared to higher order assemblies and monomers, following DNA hybridisation and subsequent separation/purification of the resultant assemblies. This scheme is able to achieve assembly of larger asymmetric nanoparticles, as well as incorporate different materials into discrete, well-defined higher-order structures, using only two complementary 100-base long, thiol functionalised DNA strands, thanks to the following steps:

The as-synthesised nanoparticles, which intrinsically have different physico-chemical properties due to their differing synthetic conditions and ligands/surfactants, are converted into stable DNA-functionalised monomers (Scheme 1(a)). This is made possible by the use of a short alkyl-PEG ligand that drastically increases the colloidal stability of the different particles, as described in details in Section 2.5 of this manuscript. This step involves (i) attachment of DNA strands onto the surface of the nanoparticles, (ii) subsequent ligand exchange to increase their colloidal stability, and (iii) purification of the reactive monomers, including those containing exactly one DNA per particle, using electrophoresis.

The assembly of the as-prepared monomers with complementary DNA sequences to achieve the desired structure is followed by electrophoretic purification (Scheme 1(b)). The output of the assembly scheme is determined by the DNA coverage of the different nanoparticles. Hetero-dimers are preferentially produced using both particles with a low DNA coverage on average (less than one DNA/particle on average), so that they can be subsequently separated from other structures using electrophoresis. Homostructures (dimers, trimers, tetramers…) are produced using particles attached to slightly more than one DNA on average.

Conversely, if some particles have a high DNA coverage, they can be used to achieve a core–satellite assembly. In the latter case, 10 nm gold spheres attached to a single DNA strand are preferred as satellites in order to avoid cross-hybridisation between cores. The advantages of this approach include its combinatorial nature, flexibility and high purity products.

The formation of the different plasmonic assembly types in high yield requires that particles are tethered to a controlled number of DNA strands, notably to prevent higher order oligomerisation (uncontrolled aggregation), which is difficult for non-spherical or large particles (> 20 nm). In general, controlling a priori the coverage of thiolated DNA on larger nanoparticles is highly challenging. It strongly depends on the particle material, its colloidal concentration, surface chemistry and surface coverage, surface electrostatic charge and the affinity difference of the existing surfactant/ligand compared to the thiol group. This means that, in general, even for known concentrations (or ratios) of nanoparticles and DNA, the resultant surface coverage of the DNA on the nanoparticle cannot be reliably predicted across different colloidal samples

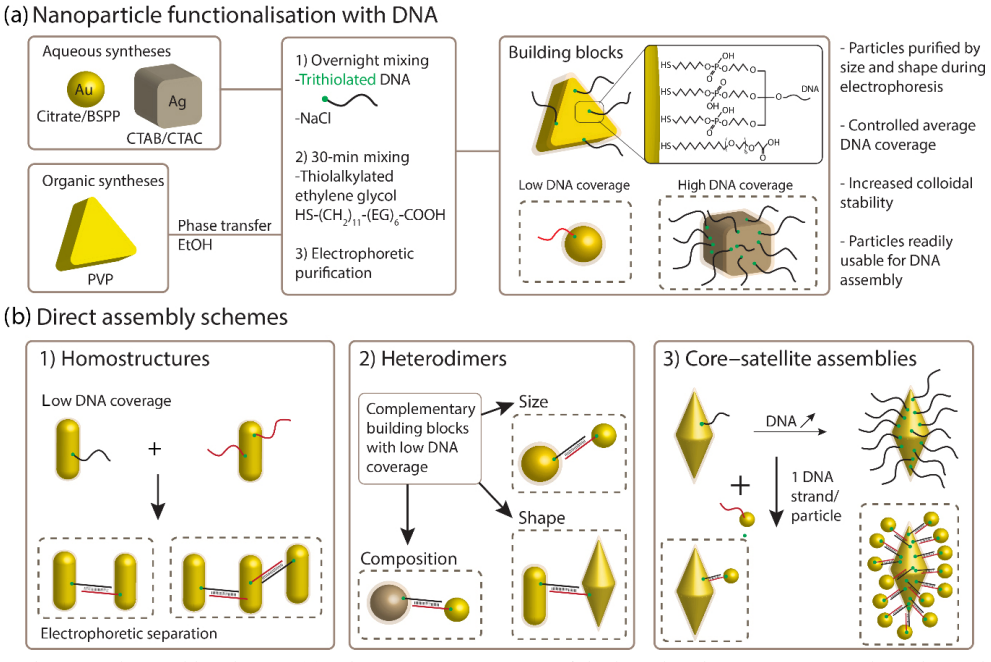

Scheme 1 Ligand exchange and assembly schemes. (a) Schematic representation of the ligand exchange steps to produce electrophoretically purified, DNA-functionalised, and alkyl-PEG passivated plasmonic building blocks from as-synthesised nanoparticles. (b) Different DNA-directed assembly schemes.

of different materials, sizes, shapes, surface chemistry, and polydispersity. We also note that finding the nanoparticle concentration constitutes a significant challenge within itself for many (although not all) colloidal preparations. For this reason, we devised an approach which is independent of the particle concentration, and which relies on the DNA functionalised particle electrophoretic mobility to estimate the DNA coverage on the particles. This allows for the formation of high-purity assemblies across many colloidal preparations, including those for which it is prohibitively difficult (or uses methods which destroy a significant proportion of the colloid) to calculate the particle concentration. This endows the method with maximum versatility. To do so, we rely on qualitatively estimating the DNA coverage using the mobility change observed via electrophoresis upon the functionalisation of the surface with different numbers of DNA strands (Figs. 1(a), 3(a), and 4). The electrophoretic mobility of nanoparticles is altered upon the binding of DNA strands to the particle surface as it changes both the hydrodynamic volume (which increases, resulting in decreased mobility) and negative charge (which increases, resulting in increased mobility). The hydrodynamic volume is then changed as a function of the number of DNA strands bound to the nanocrystal surface. Using the change in electrophoretic mobility to estimate DNA surface coverage rather than relying on the separation of nanoparticles containing just one or two DNA strands allows extension of the method to larger particles. Moreover, this technique exploits the already known advantages of electrophoresis, such as shape separation [59, 60] (see Figs. 1(a), 4(a), and 4(b), Figs. S1 and S2 in the Electronic Supplementary Material (ESM)) and particle purification from reactants (excess DNA and surfactants/ligands). In the following step, we assemble particles with a wide range of DNA coverage and electrophoresis of the assembly products enables us to determine the optimised DNA coverage that produces the highest yield of the desired structure (Fig. 1(a)).

2.2 Homostructures

By mixing building blocks containing complementary DNA strands and similarly low DNA coverage, plasmonic homostructures containing different nanoparticle morphologies are formed in solution and obtained in high purity after electrophoretic purification. Examples of rods, spheres, bipyramids, and triangles are shown in Fig. 1. Optimal conditions to produce mainly the desired homostructures are determined by hybridising particles with a very low DNA coverage (as established by the nanoparticle electrophoretic mobility) and sequentially using particles attached to an increasing number of DNA strands. Optimal DNA coverage results in an electrophoretic gel showing distinct bands corresponding to homo-assemblies in high purity (Fig. 1(a), Figs. S3 and S4 in the ESM). Statistical analysis of the particle orientation within the deposited dimers shows that the nanoparticles within the nanoassemblies preferentially orient to form assemblies with specific nanoparticle arrangements (Figs. 1(b)–1(f), Figs. S5–S11 in the ESM). For example, the deposited gold nanorod dimers are aligned side-by-side over 90% of the time, whereas only 3% deposit end-to-end (Fig. 1(b)). This side-by-side configuration is known to generate chiral plasmonics [61]. The same result is observed for bipyramid and asymmetric triangle assemblies (Figs. 1(e) and 1(f)).

We propose that, upon deposition, the structures orientate to maximise their van der Waals contact surface between the particles, generally aligning along the nanocrystal sides (as opposed to vertices/tips). When deposited, these structures show very small interparticle distances, such that they are essentially in primary ligand contact with the metal structures separated then by the thickness of the ligand shell [21, 58]. The small interparticle separation favours coupling of the nanocrystal plasmon resonances. Dimers composed of bipyramid building blocks preferentially form two structural morphologies, V-shaped and side-to-side, which account for 97% of the dimer morphologies. Trimers mostly form four different shapes with at least two particles in a V-shape; the position of the third particle determines the overall shape of the structure. The nanotriangle dimers predominantly form an edge-to-edge assembly orientation (88%). For rod trimers and tetramers, we also observe many three-dimensional (3D) structures with rods deposited on top of the others. These structures have

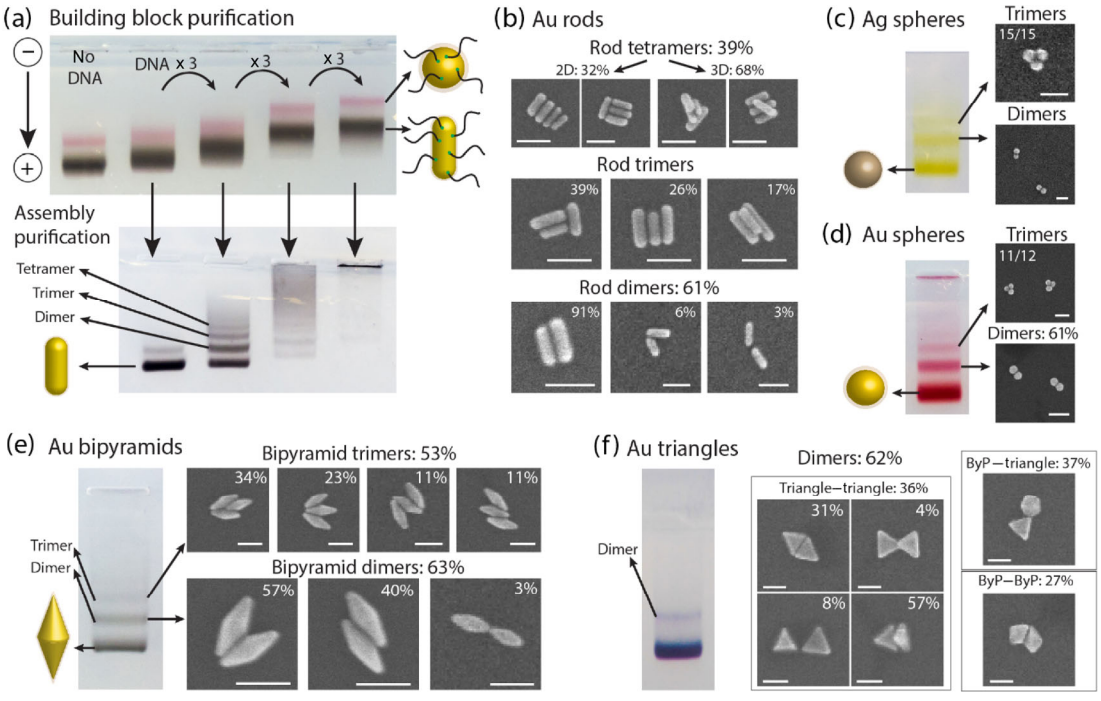

Figure 1 Self-assembled homostructures. (a) Electrophoretic separation of gold nanorods (brown bands) and gold nanospheres (pink bands - synthesis byproducts) without DNA (left band) or mixed with different amounts of DNA (3-fold increase between two consecutive columns) (top gel). An identical gel is obtained using the complementary DNA (not shown). Electrophoretic purification of the self-assembly using the DNA-conjugated nanorods extracted from the top gel (bottom gel). (c)–(f) Electrophoretic purification of (c) Ag spheres, (d) Au spheres, (e) Au bipyramids, and (f) asymmetrical triangle homo-assemblies. (b)–(f) SEM images of the homo-assemblies extracted from the corresponding gel band. They show the most commonly found structure arrangements. (f) The as-synthesised colloidal solution of nanotriangles contains byproducts (ByP) in 25% shape yield that cannot be size-separated. Consequently, the corresponding dimer assembly yields three types of structures, including some heterostructures (triangle–triangle, ByP–triangle, and ByP–ByP). Triangle–triangle structure in the bottom right corresponds to any dimer with at least one triangle standing up. (b)–(f) The percentage given after each structure name corresponds to the calculated yield of the deposited structures. The percentage on each SEM image corresponds to the yield of the deposited arrangement. Asterisks indicate that the SEM sample was too dilute to provide a yield. Scale bars: 50 nm.

potential to exhibit circular dichroism at the single structure level [62].

It is also possible that these morphologies exist to some degree in the assemblies in solution. However, as the alkyl-PEG used has been shown to lead to extended DNA strands in nanoparticle assemblies in solution [63], the interparticle distance in solution is likely to be larger. Modulating the length of the DNA could therefore allow the control of this distance.

We note that the yields quoted for the formation of a given species (for example, bipyramid dimers) are the minimum yield as some decomposition of the assemblies is observed upon deposition onto the substrate. This is presumably due to strong local forces encountered during drying of the sample such as capillary forces, solvent pinning and Van der Waals attraction to the substrate. Consequently, it is likely that the purity of the assembly in solution is higher than indicated. Increasing the DNA bond strength after the assembly, via silica-embedding [64] or silver-embedding [65], could reduce the assembly decomposition.

2.3 Heterodimers

Heterodimers are made of two particles of different size, shape or material. Such particles often have different electrophoretic mobilities and purifying hetero-assemblies larger than dimers is therefore complex because they do not produce distinct bands as homo-assemblies do.

For example, a trimer made of two different objects A and B could be made in the ratio 1:2 or 2:1 of A and B, resulting in two bands of different mobilities or a single larger but blurred band. Therefore, we developed two different approaches focusing on producing heterodimers in high purity (Fig. 2 and Fig. S12 in the ESM).

The first approach relies on the conjugation of small spheres containing one DNA strand per particle (see Fig. 4(c)) to a central particle functionalised with a low DNA coverage. If the volume difference between the two particles is relatively low, their assembly into dimers and trimers produces distinct bands. For example, Ag–Au heterodimers with particles of different sizes and Au rod-sphere heterodimers, known for their two-photon photoluminescence [66, 67] and chiroptical response [68] are shown in Figs. 2(a) and 2(b) respectively. The low DNA coverage on the larger particle is achieved as outlined above for homodimers, while for the smaller (up to 15 nm particles for 100-base pair long DNA), purified samples of nanoparticles containing a precise number of DNA strands are used.

An alternative approach employs only large particles with a very low DNA coverage, which is less than one DNA per particle on average. As a large number of the particles have no DNA attached, the self-assembly yield is low. However hybridisation of particles with one DNA/particle gives dimers which can be well identified and purified from bare nanocrystals by electrophoresis. The extraction and re-concentration of the electrophoretic band gives these structures in high dimer purity (see Figs. 2(c)–2(e) showing the three possible dimers made of a bipyramid, a rod, or a sphere). As for the homostructures, the nanoparticles within the heterodimers orient to maximise their interparticle contact (Figs. S13–S18 in the ESM). For rod–sphere dimers, the position of the sphere is dependent on the size of the sphere. It is placed at the tip of the rod from 42% to 6% when the sphere diameter increases from 10 to 40 nm (Figs. 2(b)–2(c)). This trend was also observed in sphere–rod dimer constructed

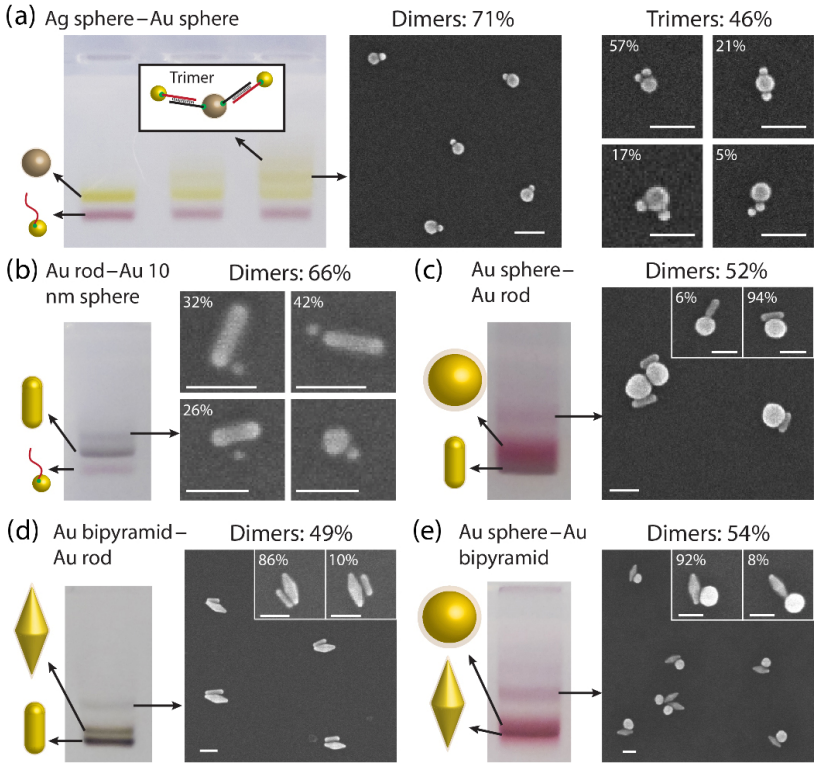

Figure 2 Self-assembled heterodimers. (a) Electrophoretic purification of the assembly products of monoconjugated gold 10 nm spheres mixed with silver spheres either without DNA (left column) or with an increased coverage of the complementary DNA (see Fig. 4(d)). (b)–(e) Electrophoretic purification of gold (b) rod–10 nm sphere, (c) sphere–rod, (d) bipyramid–rod, and (e) sphere–bipyramid dimers. (a)–(e) SEM images of the content of the designated bands. The percentage given after each structure name corresponds to the yield of the deposited structures. (a)–(b) SEM images and (c)–(e) insets correspond to the most commonly found structure arrangements presented with their relative yields. Scale bars: 50 nm.

with electrostatic interactions [69]. For dimers made with at least one bipyramid, the other particle, rod or sphere, sits on the edge of the bipyramid forming a V-shaped structure in respectively 86% and 92% yield.

2.4 Core–satellite assembly

The flexibility of the approach outlined above is highlighted by the ability to also form core–satellite structures where the number of satellites can be systematically varied. These structures, used as sensitive refractive index sensors [70] and for their SERS signals [71], consist of a central nanocrystal with very high DNA coverage, and satellite nanocrystals which are functionalised and purified to have one DNA strand per particle.

Figure 3(a) shows the agarose gel for gold bipyramids functionalised with increasing amounts of DNA. The bipyramids act as cores and from the gel it is possible to estimate qualitatively the density of the DNA attachment on the bipyramid, thereby giving a means of control over the satellite nanoparticle coverage on the core. Hybridisation of the cores with an excess of satellite nanocrystals and subsequent electrophoresis allows isolation of core–satellite structures with varying satellite coverage. As the satellite coverage increases around the core nanocrystal, the mobility of the core–satellite decreases in the gel (Fig. 3(a)). A gradual colour change (from grey to grey/pink) in this band and a concomitant decrease in the intensity of the unreacted satellite band as the satellite coverage on the bipyramid increases are observed, as would be expected. Electron microscopy of the isolated and purified core–satellite bands shows high yields of each structure, with satellite coverage varying from 1 to over 20 satellites on average (structures a–i on Figs. 3(a)–3(c) and Figs. S19–S28 in the ESM). Figure 3(c) shows a linear increase of the number of satellites when the DNA amount increases until reaching a plateau, corresponding to a saturation of the number of satellites (around 22 per core). The slope of the linear trend shows that when the DNA amount is doubled, the number of satellites goes through a 1.77-fold increase; which is to be compared with a 2-fold increase of an ideal case. This increase is therefore very reasonable given that it is likely not all the DNA hybridises with satellites due to steric hindrance, and that the sphere count is a minimum estimate as a number of satellites are positioned underneath the core and some are detached from the core upon deposition. Moreover, upon drying on the substrate, the spheres deposit below and on the side of the bipyramids whereas in solution they surround the core. This morphological change upon deposition is a way to produce asymmetric assemblies from isotropically-functionalised building blocks.

The flexible and robust nature of this DNA-based assembly approach was demonstrated by purifying core–satellites using cores of different shapes, materials, and sizes (see Figs. 3(d)–3(f) and Figs. S29–S32 in the ESM). Incorporation of semiconductor nanocrystals into the DNA-based assembly is also possible using the approach outlined (Fig. 3(f) and Fig. S33 in the ESM). The key challenge of fabricating these hybrid structures is to embed a material with a very different surface chemistry into the assemblies. Semiconductor nanocrystals are typically synthesised in organic solution with surfactants containing long alkyl chains. Following ligand exchange and concomitant phase transfer to aqueous solution using phosphonoacetic acid (PsAA), the surface of $CdSe(CdS)_4$ nanocrystals is functionalised with a high density of monothiolated DNA strands (see Fig. 4(e)). Conjugating the $CdSe(CdS)_4$ nanocrystals with satellite monoconjugated Au nanoparticles then results in the formation of core–satellite structures. On the top transmission electron microscope (TEM) image of Fig. 3(f), the "lighter" central nanocrystal is the $CdSe(CdS)_4$ nanocrystal, while the

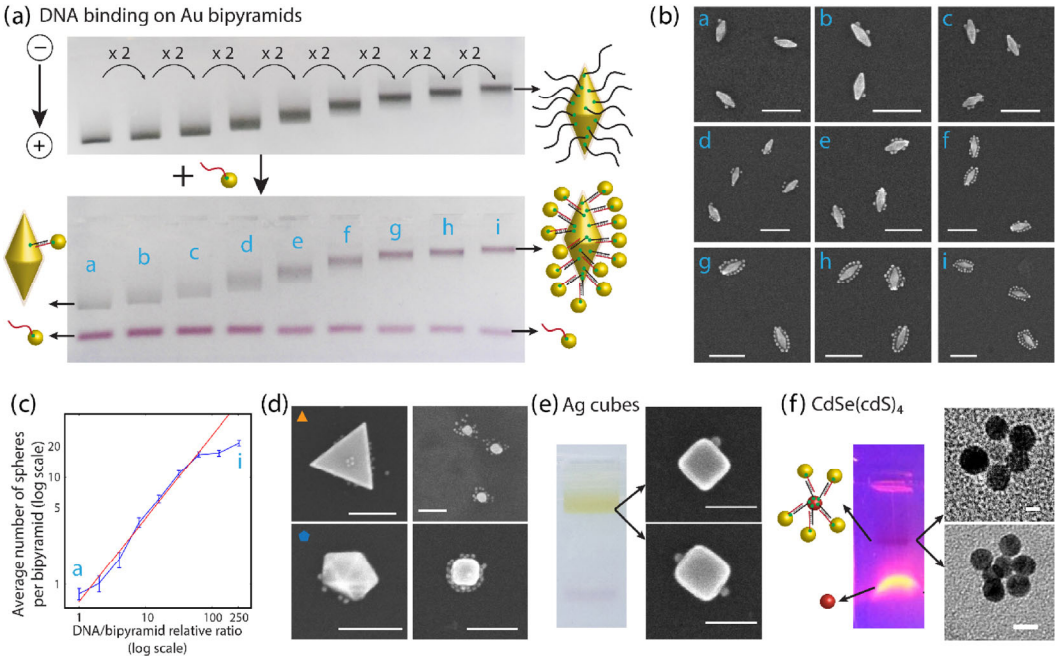

Figure 3 Core–satellite assembly. (a) (Top gel) electrophoretic purification of purified gold bipyramids mixed with different amounts of DNA (2-fold increase between consecutive columns from left to right). (Bottom gel) purification of the DNA-tethered bipyramids from panel (a) mixed with complementary mono-functionalised 10 nm gold spheres. Letters a–i indicate the assembled structure bands (upper bands). The pink lower bands correspond to the unreacted mono-functionalised spheres. (b) SEM images of the bands a–i. Scale bars: 100 nm. (c) Maximum likelihood estimates (with the 95% confidence intervals) of the means of the distributions of the number of spheres (satellites) attached to individual bipyramids (core). (d) SEM images of different gold core–satellite assemblies with a symmetrical triangle (top left), decahedron (bottom left), 40 nm spheres (top right) and cubes (bottom right) as gold cores, and mono-functionalised spheres as satellites. Scale bars: 100 nm. (e) Electrophoretic purification of silver cube–gold sphere assembly. SEM images of a silver attached to a single (top) or two (bottom) gold spheres. Scale bars: 50 nm. (f) Electrophoretic purification of $CdSe(CdS)_4$ sphere–gold sphere assembly. TEM images of two different configurations. Scale bar (top): 5 nm. Scale bar (bottom): 10 nm.

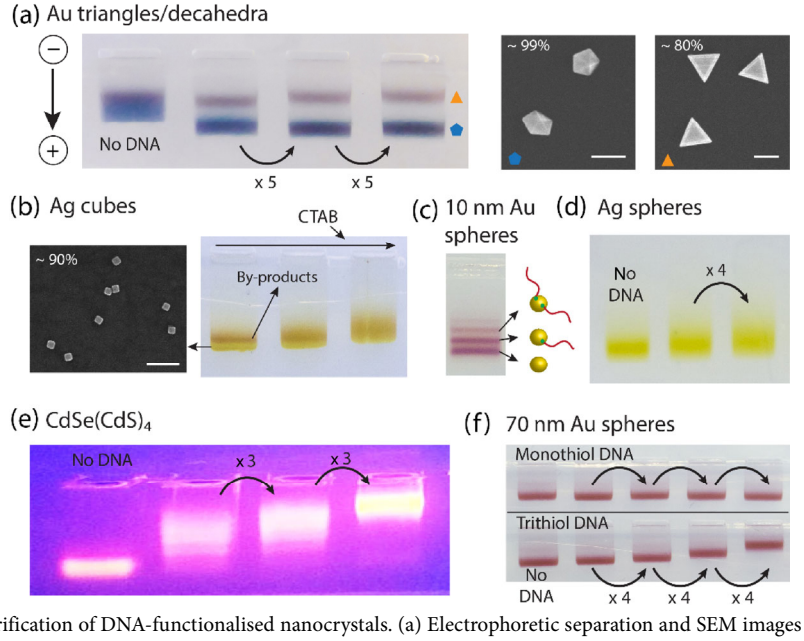

Figure 4 Electrophoretic purification of DNA-functionalised nanocrystals. (a) Electrophoretic separation and SEM images of gold symmetrical triangles (brown bands - right SEM image) and gold decahedra (blue bands in the left SEM image) without DNA (left band) or mixed with different amounts of DNA. Scale bars: 100 nm. (b) Purification gel of silver cubes of different initial CTAB concentrations (decreasing from left to right) and mixed with the same amount of DNA. SEM image of the purified silver cubes (pale yellow band). Scale bar: 200 nm. (c) Electrophoretic separation of 10 nm gold spheres tethered to a single DNA strand. (d)–(e) Electrophoretic purification of (d) silver spheres and (e) $CdSe(CdS)_4$ quantum dots without DNA (left column) or mixed with different amounts of DNA. (f) Comparison of 70 nm gold nanospheres without DNA (left columns) or mixed with different amounts of monothiol (upper gel) or trithiol (lower gel) DNA strands.

bottom TEM image highlights the 3D nature of the assemblies, showing stacked satellite nanocrystals (with the core obscured by the top nanoparticles).

To demonstrate that the assembly schemes described are driven by the DNA, we used the core–satellite structures and compared the self-assembly of DNA-coated spheres with satellites that were mono-functionalised with either the complementary or a non-complementary DNA strand of the same length (see Fig. S32 in the ESM). Both electrophoresis and electron microscopy confirmed that only complementary

strands produced core–satellite assemblies.

2.5 Preparation of functionalised particles

The crucial enabling step to form the assemblies shown above is the successful functionalisation of the starting nanoparticles, which can have different physico-chemical properties depending on the surface atoms, synthesis route and surface adsorbates/surfactants. The advantage of the approach outlined is its ability to adjust the varying surface chemistry of the starting nanocrystals to allow a uniform surface following the DNA functionalisation.

The as-synthesised nanoparticles are prepared for the DNA binding either by decreasing the density of the surface ligand using consecutive centrifugations (for hexadecyltrimethylammonium bromide (CTAB) and polyvinylpyrrolidome (PVP)-coated nanoparticles) or by a ligand exchange (citrate to bis-(p-sulfonatophenyl)phenylphosphine (BSPP) or tetradecylphosphonic acid/oleylamine/trioctylphosphine/octanethiol to PsAA for $CdSe(CdS)_4$). PVP-coated particles produced in N,N-dimethylformamide (DMF) are centrifuged and re-dispersed twice in ethanol and kept concentrated. Once prepared, particles are mixed overnight with thiolated DNA and salt. Tween 20 is used with CTAB particles as it favours the PEG passivation [72, 73]. Finally, they are passivated by a thiolated, carboxy-terminated short chain alkyl-PEG ligand for 30 min before electrophoretic purification. This ligand has been shown to very efficiently penetrate the hydrophobic CTAB layer [74], reduce surface ligand exchange with proteins [75] and confer the particles with a high chemical stability [76, 77]. It allows the DNA-based assembly to be carried out without aggregation of the sample and enables an electrophoretic purification of the products.

Generally, to verify that DNA functionalisation has occurred and to quantify the relative extent of DNA surface coverage for any new particle type, we use an increasing amount of DNA and a reference as a control. Because the number of strands attached onto the particles should follow a Poisson distribution, for low DNA/particle ratios we observe either distinct bands if the particle is small enough (Fig. 4(c)) or a band broadening with little band shift compared to the reference (Fig. 4(d)). Higher coverage of DNA strands then shifts the corresponding bands until reaching a plateau, which corresponds to the saturation of the surface (see top gel in Fig. 3(a)).

Importantly, this particle preparation can be carried out using mono- or tri-thiolated DNA. However, we observed that a large excess of alkyl-PEG tends to remove monothiolated DNA from the particle surface. Figure 4(f) shows no electrophoretic mobility change is observed for particles prepared with monothiolated and an excess of alkyl-PEG, which differs from particles prepared in the same way but with a trithiolated DNA of the same length. It is possible that a self-assembled monolayer of the alkyl-PEG displaces the monothiolated DNA which is less strongly bond to the surface than the trithiolated DNA (Scheme 1(a)). As shown with the case of $CdSe(CdS)_4$ particles, a partial passivation of the surface with the alkyl-PEG still confers particles with enough colloidal stability in water to perform a DNA self-assembly.

Due to the alkyl-PEG passivation, all the different particles are negatively charged, DNA-functionalised and have an increased colloidal stability. These particles (Table 1) represent a comprehensive library of nanoparticle building blocks as any particles with complementary strands could self-assemble into plasmonic molecules that can be purified using electrophoresis.

Contrary to other surface chemistries, CTAB-stabilised particles require an initial optimisation step to determine the CTAB concentration and enable the DNA conjugation onto the surface: an excessively low CTAB concentration (below the critical micelle concentration) may cause colloidal aggregation, whereas an excessively high concentration prevents the DNA from attaching to the particle surface. This optimisation step consists of mixing particles at different CTAB concentrations and a unique DNA amount. Decreasing the CTAB concentration progressively enables the DNA to bind onto the particle surface, resulting in a band shift upon electrophoresis (Fig. 4(b)).

Although conjugating particles with DNA often tends to decrease their mobility (Figs. 4(b)–4(f)), the opposite effect can be observed (Fig. 4(a)). Importantly, this particle-dependent behaviour upon DNA conjugation can enable the shape separation of particles. For example, unfunctionalised gold decahedra and triangles (truncated triangular bipyramids), both products of the same synthesis, exhibit identical mobilities. DNA functionalisation of the particles results in a differential change in electrophoretic mobility for the two different morphologies (Fig. 4(a)), facilitating their separation. In

Table 1 Summary of the 12 different as-synthesised nanoparticle types, i.e. of different materials, shapes, and sizes, and their corresponding surface chemistry. The table rows distinguish the 10 different chemical syntheses performed. Shape yields of the nanoparticle colloids were calculated by electron microscopy before and after purification, if performed

Synthesis number	Synthesis product	Size	Shape yield	Surface chemistry	Purification technique	Final shape yield
1	Au spheres	10 nm diameter	> 99%	Citrate		
2	Au spheres	40 nm diameter	> 99%	Citrate		
3	Au rods	40 nm length, 15 nm width	50%	CTAB	Electrophoresis	> 90%
	Au spheres	40 nm diameter	40%	CTAB	Electrophoresis	> 90%
4	Au bipyramid	60 nm length 22 nm width	50%	CTAC	as in Ref. [81]	95%
5	Au asymetrical triangles	55 nm EL	75%	CTAB		
6	Au decahedra	55 nm EL	60%	PVP in DMF	Electrophoresis	> 99%
	Au symmetrical triangles	132 nm EL	35%	PVP in DMF	Electrophoresis	80%
7	Au cubes	40 nm EL	60%	CTAB		
8	Ag spheres	23 nm diameter	> 99%	CTAB		
9	Ag cubes	45 nm EL	40%	CTAB	Electrophoresis	80%
10	$CdSe(CdS)_4$ spheres	8.5 nm diameter	> 99%	TDPA/OA/TOP/OT		

The length of Au bipyramids corresponds to the projected tip-to-tip distance; EL: edge length.

contrast, silver cubes could not be separated as cleanly from their byproducts once they were attached to DNA strands as the two corresponding electrophoretic bands merged (Fig. 4(b)). The reason for this shape-dependant behaviour is still unclear.

3 Conclusions

Using only a single thiolated DNA oligomer and a short thiolated alkyl-PEG ligand we transform a vast library of as-synthesised nanocrystals of different sizes, shapes, and materials into various well-defined, discrete assemblies. The library encompasses metal (gold and silver) as well as semiconductor (CdSe) nanoparticles for the formation of hybrid structures. By tuning the DNA coverage on different nanocrystals, we are able to direct the self-assembly into specific assemblies that could be purified by electrophoresis. Upon deposition, the nanoparticles adopt specific orientations within the assemblies which maximise the surface contact between particles and result in good morphology purity for the assemblies. This systematic effect can be exploited to avoid the need for the use of large origami templates to form desired structures.

Although we only used a single set of complementary DNA strands in this study, more complex structures could be obtained using other sets of DNA strands. The approach is applicable for nanocrystals which have a strong binding affinity to thiol groups. The very small interparticle distances in the deposited structures have the potential to provide strong optical responses at the nanoparticle level, thanks to plasmon (or plasmon/exciton) coupling.

4 Experimental

4.1 Materials

Gold(III) chloride trihydrate ($HAuCl_4{\cdot}3H_2O$) (≥ 99.9%), silver nitrate ($AgNO_3$) (≥ 99%), cadmium oxide (CdO) (99%), selenium powder (Se) (99.00%), sulfur (S) (≥ 99.99%) sodium borohydride ($NaBH_4$) (≥ 99%), L-ascorbic acid (≥ 99%), tannic acid, tri-sodium citrate dihydrate (≥ 98.5%), hexadecyltrimethylammonium chloride (CTAC) (≥ 98.0%), PVP (M_W 10,000 and M_W 40,000), Tween 20, octadec-1-ene (ODE) (technical grade, 90%), oleylamine (technical grade, 70%), octanethiol (≥ 98.5%), trioctylphosphine oxide (90%), PsAA (98%), trioctylphosphine (90%), and bis-(p-sulfonatophenyl)phenylphosphine (BSPP) (97%) were purchased from Sigma-Aldrich. CTAB (98%), chloroform (high pressure liquid chromatography (HPLC) grade), acetone (analytical reagent (AR) grade), and methanol (AR grade) were purchased from Ajax Finechem. Potassium carbonate was purchased from Merck and tetramethylammonium hydroxide (TMAOH) (25% w/w in methanol) was purchased from AlfaAeser. Thiolated ethylene glycols HS-$(EG)_6$-CH_3 and HS-C_{11}-$(EG)_6$-OCH_2-COOH were purchased from Polypure (Norway) and Prochimia Surface (Poland), respectively.

PAGE-purified trithiolated DNA sequences were purchased from Fidelity Systems, Inc. (USA). Monothiolated DNA sequences (purified via desalting) were purchased from Integrated DNA Technologies (NDT) (Singapore). The oligomers were 100-mers with the following sequences:

Monothiolated DNA

AM1: 5'-thiol-GTTAAGACGGCACTACCATTCA AATTA CAAGGATGAGGCACGCTCACGGTGCTCGCAGACATGA GTTAGCGAAGCGGTACTCCAGCTCTAGGTAGCTCCC-3'

AM1': 5'-thiol-GGGAGCTACCTAGAGCTGGAG TACCG CTTCGCTAACTCATGTCTGCGAGCACCGTGAGCGTGC CTCATCCTTGTAATTTGAATGGTAGTGCCGTCTTAAC-3'

Trithiolated DNA

AT1: 5'-trithiol-TTTTCTCACTAAGATCGATAGA GCGA TTGTGATATTTCAAGCGGTACTCCAGCTCTAGGTAGCT CCCTTTCCAATCAGCTTATGTGAGCGCCTGCCCATG-3'

AT1': 5'-trithiol-TTTCATGGGCAGGCGCTCACA TAAGCT GATTGGAAAGGGAGCTACCTAGAGCTGGAGTACCGCT TGAAATATCACAATCGCTCTATCGATCTTAGTGAGA-3'

All chemicals were used as received without further purification. Ultrapure water (18.2 MΩ, Milli-Q) was used for all the procedures.

4.2 Nanocrystal synthesis

Nanocrystals were synthesised according to literature reports as follows. Monodisperse small gold nanospheres were synthesised according to the method of Piella et al. [78], gold nanospheres according to the method of Lu et al. [79], gold nanorods according to the method of Nikoobakht and El-Sayed [80], gold bipyramids according to the method of Li et al. [81], gold asymmetrical triangles according to the method of Scarabelli et al. [82], and gold triangles and decahedra according to the method of Sanchez-Iglasias et al. [83]. Silver cubes were synthesised according to the method of Lin [84].

The synthesis of gold nanocubes was based on the procedures reported previously [85–87] with slight modifications. Briefly:

(1) Gold seeds: An aqueous solution of $HAuCl_4$ (0.025 mL, 0.050 M) was added to an aqueous solution of CTAB (3.75 mL, 0.10 M). The resultant solution was stirred for at least 5 min. Upon rapid addition of freshly prepared $NaBH_4$ (0.30 mL, 0.025 M, at room temperature in ultrapure water) into the mixture under vigorous stirring, the initially yellow-orange solution became light brown. The resultant solution was stirred for 15 min. The final seed dispersion was kept at 30 ± 1 °C in a thermostated water bath for at least 45 min before further use.

(2) Growth of gold nanocubes: The growth solution was prepared as follow: an aqueous solution of $HAuCl_4$ (0.08 mL, 0.050 M) was added to an aqueous solution of CTAB (3.20 mL, 0.10 M) and ultrapure water (16 mL). Upon addition of a solution of ascorbic acid (1.90 mL, 0.10 M), the solution changed from a golden color to colorless. The gold seed solution was diluted by a factor of 10 for further use. The growth of nanocubes was initiated by adding 0.002 mL of the diluted gold seed solution into the growth solution. The final dispersion was kept at 30 ± 1 °C in a thermostated water bath for 12 h.

Core–shell semiconductor nanocrystals $CdSe(CdS)_4$ were synthesised and subsequently shelled according to reported methods [88–90].

4.3 Ligand exchange

For citrate particles, a BSPP ligand exchange was performed to increase their colloidal stability while still allowing the DNA binding [50, 54, 63]. CTAB and CTAC passivated nanoparticles were washed by centrifugation and stored in 1 mM CTAB or CTAC concentration. PVP passivated decahedra/triangles synthesised in DMF were transferred and reconcentrated in ethanol. $CdSe(CdS)_4$ were phase transferred via PsAA ligand exchange.

A dispersion of the $CdSe(CdS)_4$ in chloroform (13 μM, 1.00 mL) was added to a methanolic solution of PsAA (0.1 M, 1.00 mL) with pH adjusted to pH 8 using TMAOH in methanol (25% w/w solution). The mixture was sonicated for 1–2 min. Following addition of water (1.00 mL), the $CdSe(CdS)_4$ nanoparticles migrate to the aqueous layer upon sonication, leaving a colorless organic layer. The aqueous layer containing the $CdSe(CdS)_4$ was collected and washed twice by precipitating

the nanoparticles via addition of acetone (~ 5–10 mL). The precipitate was centrifuged and the pellet redispersed in water to remove excess of PsAA.

4.4 Preparation and purification of nanoparticle–DNA conjugates

General approach: After the ligand exchange, particles were kept relatively concentrated (strongly coloured) but the concentrations were not precisely known. To overcome this, several aliquots of particles were mixed with different DNA concentrations and electrophoresis was used to purify the DNA-attached particles and estimate the DNA coverage. The general protocol to bind DNA onto all the different particles was as follows: 3 μL of concentrated particles were incubated overnight with NaCl and thiolated DNA at room temperature in a total volume of 15 μL (concentrations are detailed below). Thiol-PEG (only used with 10 nm Au spheres) or thio-alkyl-PEG passivation of the nanoparticle surface was achieved by incubation of the particles for 30 min in an excess of PEG (1 μL of concentrated PEG; ~ 100,000–500,000 molar excess with respect to the particle concentration) prior to electrophoretic purification. In all following electrophoreses, Ficoll 400 (20% solution) was added in a 1:5 volume ratio as a loading buffer and agarose gels were run at 8 $V \cdot cm^{-1}$ for about 35–45 min with 0.5× tris-borate-ethylenediaminetetraacetic acid (TBE) as the running buffer. The extraction procedure was carried out following published protocols [19, 54] and samples were re-concentrated by centrifugation (final volume of ~ 10–50 μL).

Nanoparticles attached to a single DNA strand (10 nm Au spheres): To prepare monoconjugated particles, a 10 nm gold nanoparticle solution was mixed with a 1× – 3× excess of trithiolated DNA strands with 6 mM BSPP and 70 mM NaCl final concentrations. Thiol-PEG and 3% agarose gel were used.

DNA binding to large nanoparticles: For 40 nm BSPP spheres, the procedure was performed according to existing literature [63, 77]. In brief, DNA-functionalised gold nanoparticles were obtained by incubating BSPP-functionalised gold nanoparticles with different volumes of trithiolated DNA strands in a 12 mM NaCl and 1.5 mM BSPP solution. Alkyl-PEG and 1.5% agarose gel were used.

As detailed in the main text, CTAB/CTAC particles require an optimisation step to determine a surfactant concentration range which enables the DNA binding without precipitation of the particles. It is performed by varying the surfactant concentration at a given DNA concentration. Final CTAB/CTAC concentrations could range from 0.05–1 mM. Once determined, Au particles were mixed overnight in a 66 mM NaCl and 6 mM BSPP solution and with 1 μL of a solution of Tween 20 (stock solution diluted 10 times). For Ag particles, the same reactants were used but the NaCl concentration used was lower (around 10 mM to minimise the formation of AgCl) and the CTAB concentration was higher (0.5–1 mM). As a higher CTAB concentration hindered the DNA binding to the particles, we used higher DNA concentrations for Ag particles than for Au particles to obtain approximately the same coverage.

PVP particles synthesised in DMF were centrifuged and redispersed twice in ethanol and kept concentrated. Using particles dispersed in ethanol (3 μL in a total of 15 μL) did not affect the DNA binding.

3 μL of $CdSe(CdS)_4$ (19.6 μM) were mixed with mono-thiolated DNA (100 μM, 10 μL) in the presence of BSPP (90 mM, 1 μL) and at a 100 mM NaCl concentration and allowed to incubate for 24 h. The $CdSe(CdS)_4$-DNA conjugates were then mixed with a 340× excess of alkyl-PEG and incubated for 30 min. The DNA-conjugated $CdSe(CdS)_4$ was purified from excess DNA via electrophoresis using a 1% agarose gel in TBE buffer with a running time of 30 min at 80 V.

4.5 Nanoparticle assembly

Assembly is performed by (1) simply mixing two types of particle with complementary DNA on the surface, (2) centrifuging to re-concentrate to a volume of approximately 20–25 μL, suitable for electrophoresis, and (3) adding NaCl to a final NaCl concentration of 100 mM. After an overnight incubation at room temperature, assemblies were purified by electrophoresis, extracted and centrifuged as previously described. The agarose gel concentration depends on the size of the particle used and varied from 0.7% when the Au symmetrical triangles were used as core (see Fig. S29(a) in the ESM) to 2% for the Ag sphere–Au sphere hetero dimers (see Fig. 2(a)).

4.6 Instrumentation

Electron microscopy was carried out at the Monash Centre for Electron Microscopy on an FEI Tecnai G2 T20 TWIN TEM using an accelerating voltage of 200 kV and an FEI Magellan 400 FEG Scanning Electron Microscope (SEM).

4.7 Microscopy sample preparation

To prepare samples for electron microscopy, 20 μL of the purified assembled structures were deposited for 10–20 min on either a holey carbon TEM grid (for TEM) or a doped silicon wafer (for SEM). The excess solution was removed and the sample washed in a bath of absolute ethanol for 15 min. The substrate was removed from the ethanol, rinsed with absolute ethanol and allowed to dry.

Acknowledgements

This work was supported by the Australian Research Council (ARC) Grants for the ARC Centre of Excellence in Exciton Science, CE170100026 and DP140103011. The authors acknowledge use of facilities within the Monash Centre for Electron Microscopy (MCEM).

Electronic Supplementary Material: Supplementary material (additional agarose gels, SEM images and statistical analysis of the assembly yields) is available in the online version of this article at https://doi.org/10.1007/s12274-020-3084-2.

References

[1] Tan, S. J.; Campolongo, M. J.; Luo, D.; Cheng, W. L. Building plasmonic nanostructures with DNA. *Nat. Nanotechnol.* **2011**, *6*, 268–276.

[2] Bouju, X.; Duguet, É.; Gauffre, F.; Henry, C. R.; Kahn, M. L.; Mélinon, P.; Ravaine, S. Nonisotropic self-assembly of nanoparticles: From compact packing to functional aggregates. *Adv. Mater.* **2018**, *30*, 1706558.

[3] Wintzheimer, S.; Granath, T.; Oppmann, M.; Kister, T.; Thai, T.; Kraus, T.; Vogel, N.; Mandel, K. Supraparticles: Functionality from uniform structural motifs. *ACS Nano* **2018**, *12*, 5093–5120.

[4] Thorkelsson, K.; Bai, P.; Xu, T. Self-assembly and applications of anisotropic nanomaterials: A review. *Nano Today* **2015**, *10*, 48–66.

[5] Langer, J.; de Aberasturi, D. J.; Aizpurua, J.; Alvarez-Puebla, R. A.; Auguié, B.; Baumberg, J. J.; Bazan, G. C.; Bell, S. E. J.; Boisen, A.; Brolo, A. G. et al. Present and future of surface-enhanced Raman scattering. *ACS Nano* **2020**, *14*, 28–117.

[6] Bidault, S.; Devilez, A.; Maillard, V.; Lermusiaux, L.; Guigner, J. M.; Bonod, N.; Wenger, J. Picosecond lifetimes with high quantum yields from single-photon-emitting colloidal nanostructures at room temperature. *ACS Nano* **2016**, *10*, 4806–4815.

[7] Kyriazi, M. E.; Giust, D.; El-Sagheer, A. H.; Lackie, P. M.; Muskens, O. L.; Brown, T.; Kanaras, A. G. Multiplexed mRNA sensing and combinatorial-targeted drug delivery using DNA-gold nanoparticle dimers. *ACS Nano* **2018**, *12*, 3333–3340.

[8] Raeesi, V.; Chou, L. Y. T.; Chan, W. C. W. Tuning the drug loading and release of DNA-assembled gold-nanorod superstructures. *Adv. Mater.* **2016**, *28*, 8511–8518.

[9] Cheng, X. J.; Sun, R.; Yin, L.; Chai, Z. F.; Shi, H. B.; Gao, M. Y. Light-triggered assembly of gold nanoparticles for photothermal therapy and photoacoustic imaging of tumors *in vivo*. *Adv. Mater.* **2017**, *29*, 1604894.

[10] Romo-Herrera, J. M.; Alvarez-Puebla, R. A.; Liz-Marzán, L. M. Controlled assembly of plasmonic colloidal nanoparticle clusters. *Nanoscale* **2011**, *3*, 1304–1315.

[11] Zhang, Y. G.; Lu, F.; Yager, K. G.; van der Lelie, D.; Gang, O. A general strategy for the DNA-mediated self-assembly of functional nanoparticles into heterogeneous systems. *Nat. Nanotechnol.* **2013**, *8*, 865–872.

[12] Maye, M. M.; Kumara, M. T.; Nykypanchuk, D.; Sherman, W. B.; Gang, O. Switching binary states of nanoparticle superlattices and dimer clusters by DNA strands. *Nat. Nanotechnol.* **2010**, *5*, 116–120.

[13] Fan, J. A.; He, Y.; Bao, K.; Wu, C.; Bao, J. M.; Schade, N. B.; Manoharan, V. N.; Shvets, G.; Nordlander, P.; Liu, D. R. et al. DNA-enabled self-assembly of plasmonic nanoclusters. *Nano Lett.* **2011**, *11*, 4859–4864.

[14] Kuzyk, A.; Schreiber, R.; Fan, Z. Y.; Pardatscher, G.; Roller, E. M.; Högele, A.; Simmel, F. C.; Govorov, A. O.; Liedl, T. DNA-based self-assembly of chiral plasmonic nanostructures with tailored optical response. *Nature* **2012**, *483*, 311–314.

[15] Slaughter, L. S.; Willingham, B. A.; Chang, W. S.; Chester, M. H.; Ogden, N.; Link, S. Toward plasmonic polymers. *Nano Lett.* **2012**, *12*, 3967–3972.

[16] Barrow, S. J.; Funston, A. M.; Wei, X. Z.; Mulvaney, P. DNA-directed self-assembly and optical properties of discrete 1D, 2D and 3D plasmonic structures. *Nano Today* **2013**, *8*, 138–167.

[17] Lermusiaux, L.; Maillard, V.; Bidault, S. Widefield spectral monitoring of nanometer distance changes in DNA-templated plasmon rulers. *ACS Nano* **2015**, *9*, 978–990.

[18] Urban, M. J.; Dutta, P. K.; Wang, P. F.; Duan, X. Y.; Shen, X. B.; Ding, B. Q.; Ke, Y. G.; Liu, N. Plasmonic toroidal metamolecules assembled by DNA origami. *J. Am. Chem. Soc.* **2016**, *138*, 5495–5498.

[19] Lermusiaux, L.; Funston, A. M. Plasmonic isomers via DNA-based self-assembly of gold nanoparticles. *Nanoscale* **2018**, *10*, 19557–19567.

[20] Lerch, S.; Reinhard, B. M. Effect of interstitial palladium on plasmon-driven charge transfer in nanoparticle dimers. *Nat. Commun.* **2018**, *9*, 1608.

[21] Mayevsky, A. D.; Funston, A. M. Control of electric field localization by three-dimensional bowtie nanoantennae. *J. Phys. Chem. C* **2018**, *122*, 18012–18020.

[22] Liu, X. L.; Liang, S.; Nan, F.; Yang, Z. J.; Yu, X. F.; Zhou, L.; Hao, Z. H.; Wang, Q. Q. Solution-dispersible Au nanocube dimers with greatly enhanced two-photon luminescence and SERS. *Nanoscale* **2013**, *5*, 5368–5374.

[23] Malachosky, E. W.; Guyot-Sionnest, P. Gold bipyramid nanoparticle dimers. *J. Phys. Chem. C* **2014**, *118*, 6405–6412.

[24] Zohar, N.; Haran, G. Modular plasmonic antennas built of ultrathin silica-shell silver-core nanoparticles. *Langmuir* **2014**, *30*, 7919–7927.

[25] Zhao, Y.; Sun, M. Z.; Ma, W.; Kuang, H.; Xu, C. L. Biological molecules-governed plasmonic nanoparticle dimers with tailored optical behaviors. *J. Phys. Chem. Lett.* **2017**, *8*, 5633–5642.

[26] Lloyd, J. A.; Ng, S. H.; Liu, A. C. Y.; Zhu, Y.; Chao, W.; Coenen, T.; Etheridge, J.; Gómez, D. E.; Bach, U. Plasmonic nanolenses: Electrostatic self-assembly of hierarchical nanoparticle trimers and their response to optical and electron beam stimuli. *ACS Nano* **2017**, *11*, 1604–1612.

[27] Gschneidtner, T. A.; Fernandez, Y. A. D.; Syrenova, S.; Westerlund, F.; Langhammer, C.; Moth-Poulsen, K. A versatile self-assembly strategy for the synthesis of shape-selected colloidal noble metal nanoparticle heterodimers. *Langmuir* **2014**, *30*, 3041–3050.

[28] Fan, Z. Y.; Tebbe, M.; Fery, A.; Agarwal, S.; Greiner, A. Assembly of gold nanoparticles on gold nanorods using functionalized poly(*N*-isopropylacrylamide) as polymeric "glue". *Part. Part. Syst. Charact.* **2016**, *33*, 698–702.

[29] Ni, S. B.; Wolf, H.; Isa, L. Programmable assembly of hybrid nanoclusters. *Langmuir* **2018**, *34*, 2481–2488.

[30] Weller, L.; Thacker, V. V.; Herrmann, L. O.; Hemmig, E. A.; Lombardi, A.; Keyser, U. F.; Baumberg, J. J. Gap-dependent coupling of Ag–Au nanoparticle heterodimers using DNA origami-based self-assembly. *ACS Photonics* **2016**, *3*, 1589–1595.

[31] Shen, C. Q.; Lan, X.; Zhu, C. G.; Zhang, W.; Wang, L. Y.; Wang, Q. B. Spiral patterning of Au nanoparticles on Au nanorod surface to form chiral AuNR@AuNP helical superstructures templated by DNA origami. *Adv. Mater.* **2017**, *29*, 1606533.

[32] Zhang, C.; Zhao, H. Q.; Zhou, L. N.; Schlather, A. E.; Dong, L. L.; McClain, M. J.; Swearer, D. F.; Nordlander, P.; Halas, N. J. Al–Pd nanodisk heterodimers as antenna–reactor photocatalysts. *Nano Lett.* **2016**, *16*, 6677–6682.

[33] Biswas, S.; Duan, J. S.; Nepal, D.; Park, K.; Pachter, R.; Vaia, R. A. Plasmon-induced transparency in the visible region via self-assembled gold nanorod heterodimers. *Nano Lett.* **2013**, *13*, 6287–6291.

[34] Lloyd, J. A.; Ng, S. H.; Davis, T. J.; Gómez, D. E.; Bach, U. Size selective adsorption of gold nanoparticles by electrostatic assembly. *J. Phys. Chem. C* **2017**, *121*, 2437–2443.

[35] Dewi, M. R.; Gschneidtner, T. A.; Elmas, S.; Ranford, M.; Moth-Poulsen, K.; Nann, T. Monofunctionalization and dimerization of nanoparticles using coordination chemistry. *ACS Nano* **2015**, *9*, 1434–1439.

[36] Liu, M.; Fang, L. L.; Li, Y. L.; Gong, M.; Xu, A.; Deng, Z. X. "Flash" preparation of strongly coupled metal nanoparticle clusters with sub-nm gaps by Ag^+ soldering: Toward effective plasmonic tuning of solution-assembled nanomaterials. *Chem. Sci.* **2016**, *7*, 5435–5440.

[37] Kumar, J.; Wei, X. Z.; Barrow, S.; M. Funston, A. M.; George Thomas, K.; Mulvaney, P. Surface plasmon coupling in end-to-end linked gold nanorod dimers and trimers. *Phys. Chem. Chem. Phys.* **2013**, *15*, 4258–4264.

[38] Borsley, S.; Flook, S.; R. Kay, E. Rapid and simple preparation of remarkably stable binary nanoparticle planet–satellite assemblies. *Chem. Commun.* **2015**, *51*, 7812–7815.

[39] Zhang, H. Y.; Cadusch, J.; Kinnear, C.; James, T.; Roberts, A.; Mulvaney, P. Direct assembly of large area nanoparticle arrays. *ACS Nano* **2018**, *12*, 7529–7537.

[40] Höller, R. P. M.; Dulle, M.; Thomä, S.; Mayer, M.; Steiner, A. M.; Förster, S.; Fery, A.; Kuttner, C.; Chanana, M. Protein-assisted assembly of modular 3D plasmonic raspberry-like core/satellite nanoclusters: Correlation of structure and optical properties. *ACS Nano* **2016**, *10*, 5740–5750.

[41] Rothemund, P. W. K. Folding DNA to create nanoscale shapes and patterns. *Nature* **2006**, *440*, 297–302.

[42] Edwardson, T. G. W.; Lau, K. L.; Bousmail, D.; Serpell, C. J.; Sleiman, H. F. Transfer of molecular recognition information from DNA nanostructures to gold nanoparticles. *Nat. Chem.* **2016**, *8*, 162–170.

[43] Schreiber, R.; Do, J.; Roller, E. M.; Zhang, T.; Schüller, V. J.; Nickels, P. C.; Feldmann, J.; Liedl, T. Hierarchical assembly of metal nanoparticles, quantum dots and organic dyes using DNA origami scaffolds. *Nat. Nanotechnol.* **2014**, *9*, 74–78.

[44] Eskelinen, A. P.; Moerland, R. J.; Kostiainen, M. A.; Törmä, P. Self-assembled silver nanoparticles in a bow-tie antenna configuration. *Small* **2014**, 10, 1057–1062.

[45] Liu, W. Y.; Li, L.; Yang, S.; Gao, J.; Wang, R. S. Self-assembly of heterogeneously shaped nanoparticles into plasmonic metamolecules on DNA origami. *Chem.—Eur. J.* **2017**, *23*, 14177–14181.

[46] Wang, M.; Dong, J. Y.; Zhou, C.; Xie, H.; Ni, W. H.; Wang, S.; Jin, H. L.; Wang, Q. B. Reconfigurable plasmonic diastereomers assembled by DNA Origami. *ACS Nano* **2019**, *13*, 13702–13708.

[47] Nykypanchuk, D.; Maye, M. M.; van der Lelie, D.; Gang, O. DNA-guided crystallization of colloidal nanoparticles. *Nature* **2008**, *451*, 549–552.

[48] Laramy, C. R.; O'Brien, M. N.; Mirkin, C. A. Crystal engineering with DNA. *Nat. Rev. Mater.* **2019**, *4*, 201–224.

[49] Kim, G. H.; Oh, J. W.; Lin, M. H.; Choe, H.; Oh, J.; Lee, J. H.; Noh, H.; Nam, J. M. Statistical modeling of ligand-mediated multimeric nanoparticle assembly. *J. Phys. Chem. C* **2019**, *123*, 21195–21206.

[50] Zanchet, D.; Micheel, C. M.; Parak, W. J.; Gerion, D.; Williams, S. C.; Alivisatos, A. P. Electrophoretic and structural studies of DNA-directed Au nanoparticle groupings. *J. Phys. Chem. B* **2002**, *106*, 11758–11763.

[51] Claridge, S. A.; Goh, S. L.; Fréchet, J. M. J.; Williams, S. C.; Micheel, C. M.; Alivisatos, A. P. Directed assembly of discrete gold nanoparticle groupings using branched DNA scaffolds. *Chem. Mater.* **2005**, *17*, 1628–1635.

[52] Aldaye, F. A.; Sleiman, H. F. Dynamic DNA templates for discrete gold nanoparticle assemblies: Control of geometry, modularity, write/erase and structural switching. *J. Am. Chem. Soc.* **2007**, *129*, 4130–4131.

[53] Fu, A. H.; Micheel, C. M.; Cha, J.; Chang, H.; Yang, H.; Alivisatos, A. P. Discrete nanostructures of quantum dots/Au with DNA. *J. Am. Chem. Soc.* **2004**, *126*, 10832–10833.

[54] Lermusiaux, L.; Sereda, A.; Portier, B.; Larquet, E.; Bidault, S. Reversible switching of the interparticle distance in DNA-templated gold nanoparticle dimers. *ACS Nano* **2012**, *6*, 10992–10998.

[55] Zanchet, D.; Micheel, C. M.; Parak, W. J.; Gerion, D.; Alivisatos, A. P. Electrophoretic isolation of discrete Au nanocrystal/DNA conjugates. *Nano Lett.* **2001**, *1*, 32–35.

[56] Claridge, S. A.; Liang, H. W.; Basu, S. R.; Fréchet, J. M. J.; Alivisatos, A. P. Isolation of discrete nanoparticle−DNA conjugates for plasmonic applications. *Nano Lett.* **2008**, *8*, 1202–1206.

[57] Busson, M. P.; Rolly, B.; Stout, B.; Bonod, N.; Larquet, E.; Polman, A.; Bidault, S. Optical and topological characterization of gold nanoparticle dimers linked by a single DNA double strand. *Nano Lett.* **2011**, *11*, 5060–5065.

[58] Funston, A. M.; Novo, C.; Davis, T. J.; Mulvaney, P. Plasmon coupling of gold nanorods at short distances and in different geometries. *Nano Lett.* **2009**, *9*, 1651–1658.

[59] Hanauer, M.; Pierrat, S.; Zins, I.; Lotz, A.; Sönnichsen, C. Separation of nanoparticles by gel electrophoresis according to size and shape. *Nano Lett.* **2007**, *7*, 2881–2885.

[60] Wang, H. Q.; Deng, Z. X. Gel electrophoresis as a nanoseparation tool serving DNA nanotechnology. *Chin. Chem. Lett.* **2015**, *26*, 1435–1438.

[61] Ma, W.; Kuang, H.; Wang, L. B.; Xu, L. G.; Chang, W. S.; Zhang, H. N.; Sun, M. Z.; Zhu, Y. Y.; Zhao, Y.; Liu, L. Q. et al. Chiral plasmonics of self-assembled nanorod dimers. *Sci. Rep.* **2013**, *3*, 1934.

[62] Wang, L. Y.; Smith, K. W.; Dominguez-Medina, S.; Moody, N.; Olson, J. M.; Zhang, H. N.; Chang, W. S.; Kotov, N.; Link, S. Circular differential scattering of single chiral self-assembled gold nanorod dimers. *ACS Photonics* **2015**, *2*, 1602–1610.

[63] Lermusiaux, L.; Bidault, S. Increasing the morphological stability of DNA-templated nanostructures with surface hydrophobicity. *Small* **2015**, *11*, 5696–5704.

[64] Jing, X. X.; Zhang, F.; Pan, M. C.; Dai, X. P.; Li, J.; Wang, L. H.; Liu, X. G.; Yan, H.; Fan, C. H. Solidifying framework nucleic acids with silica. *Nat. Protoc.* **2019**, *14*, 2416–2436.

[65] Oh, T.; Park, S. S.; Mirkin, C. A. Stabilization of colloidal crystals engineered with DNA. *Adv. Mater.* **2019**, *31*, 1805480.

[66] Garai, M.; Zhang, T. S.; Gao, N. Y.; Zhu, H.; Xu, Q. H. Single particle studies on two-photon photoluminescence of gold nanorod–nanosphere heterodimers. *J. Phys. Chem. C* **2016**, *120*, 11621–11630.

[67] Lombardi, A.; Grzelczak, M. P.; Pertreux, E.; Crut, A.; Maioli, P.; Pastoriza-Santos, I.; Liz-Marzán, L. M.; Vallée, F.; Del Fatti, N. Fano interference in the optical absorption of an individual gold–silver nanodimer. *Nano Lett.* **2016**, *16*, 6311–6316.

[68] Hao, C. L.; Xu, L. G.; Ma, W.; Wang, L. B.; Kuang, H.; Xu, C. L. Assembled plasmonic asymmetric heterodimers with tailorable chiroptical response. *Small* **2014**, *10*, 1805–1812.

[69] Pothorszky, S.; Zámbó, D.; Deák, T.; Deák, A. Assembling patchy nanorods with spheres: Limitations imposed by colloidal interactions. *Nanoscale* **2016**, *8*, 3523–3529.

[70] Prasad, J.; Zins, I.; Branscheid, R.; Becker, J.; Koch, A. H. R.; Fytas, G.; Kolb, U.; Sönnichsen, C. Plasmonic core–satellite assemblies as highly sensitive refractive index sensors. *J. Phys. Chem. C* **2015**, *119*, 5577–5582.

[71] Zheng, Y. H.; Thai, T.; Reineck, P.; Qiu, L.; Guo, Y. M.; Bach, U. DNA-directed self-assembly of core-satellite plasmonic nanostructures: A highly sensitive and reproducible near-IR SERS sensor. *Adv. Funct. Mater.* **2013**, *23*, 1519–1526.

[72] Li, J. X.; Zhu, B. Q.; Zhu, Z.; Zhang, Y. C.; Yao, X. J.; Tu, S.; Liu, R. D.; Jia, S. S.; Yang, C. J. Simple and rapid functionalization of gold nanorods with oligonucleotides using an mPEG-SH/Tween 20-assisted approach. *Langmuir* **2015**, *31*, 7869–7876.

[73] Liu, K.; Zheng, Y. H.; Lu, X.; Thai, T.; Lee, N. A.; Bach, U.; Gooding, J. J. Biocompatible gold nanorods: One-step surface functionalization, highly colloidal stability, and low cytotoxicity. *Langmuir* **2015**, *31*, 4973–4980.

[74] Schulz, F.; Friedrich, W.; Hoppe, K.; Vossmeyer, T.; Weller, H.; Lange, H. Effective PEGylation of gold nanorods. *Nanoscale* **2016**, *8*, 7296–7308.

[75] Larson, T. A.; Joshi, P. P.; Sokolov, K. Preventing protein adsorption and macrophage uptake of gold nanoparticles via a hydrophobic shield. *ACS Nano* **2012**, *6*, 9182–9190.

[76] Kanaras, A. G.; Kamounah, F. S.; Schaumburg, K.; Kiely, C. J.; Brust, M. Thioalkylated tetraethylene glycol: A new ligand for water soluble monolayer protected gold clusters. *Chem. Commun.* **2002**, *20*, 2294–2295.

[77] Lermusiaux, L.; Bidault, S. Temperature-dependent plasmonic responses from gold nanoparticle dimers linked by double-stranded DNA. *Langmuir* **2018**, *34*, 14946–14953.

[78] Piella, J.; Bastús, N. G.; Puntes, V. Size-controlled synthesis of sub-10-nanometer citrate-stabilized gold nanoparticles and related optical properties. *Chem. Mater.* **2016**, *28*, 1066–1075.

[79] Lu, X. F.; Dandapat, A.; Huang, Y. J.; Zhang, L.; Rong, Y.; Dai, L. W.; Sasson, Y.; Zhang, J. W.; Chen, T. Tris base assisted synthesis of monodispersed citrate-capped gold nanospheres with tunable size. *RSC Adv.* **2016**, *6*, 60916–60921.

[80] Nikoobakht, B.; El-Sayed, M. A. Preparation and growth mechanism of gold nanorods (NRs) using seed-mediated growth method. *Chem. Mater.* **2003**, *15*, 1957–1962.

[81] Li, Q.; Zhuo, X. L.; Li, S.; Ruan, Q. F.; Xu, Q. H.; Wang, J. F. Production of monodisperse gold nanobipyramids with number percentages approaching 100% and evaluation of their plasmonic properties. *Adv. Opt. Mater.* **2015**, *3*, 801–812.

[82] Scarabelli, L.; Coronado-Puchau, M.; Giner-Casares, J. J.; Langer, J.; Liz-Marzán, L. M. Monodisperse gold nanotriangles: Size control, large-scale self-assembly, and performance in surface-enhanced Raman scattering. *ACS Nano* **2014**, *8*, 5833–5842.

[83] Sánchez-Iglesias, A.; Pastoriza-Santos, I.; Pérez-Juste, J.; Rodríguez-González, B.; García de Abajo, F. J.; Liz-Marzán, L. M. Synthesis and optical properties of gold nanodecahedra with size control. *Adv. Mater.* **2006**, *18*, 2529–2534.

[84] Lin, X.; Lin, S.; Liu, Y. L.; Gao, M. M.; Zhao, H. Y.; Liu, B. K.; Hasi, W.; Wang, L. Facile synthesis of monodisperse silver nanospheres in aqueous solution via seed-mediated growth coupled with oxidative etching. *Langmuir* **2018**, *34*, 6077–6084.

[85] Sau, T. K.; Murphy, C. J. Room temperature, high-yield synthesis of multiple shapes of gold nanoparticles in aqueous solution. *J. Am. Chem. Soc.* **2004**, *126*, 8648–8649.

[86] Chen, H. J.; Kou, X. S.; Yang, Z.; Ni, W. H.; Wang, J. F. Shape- and size-dependent refractive index sensitivity of gold nanoparticles. *Langmuir* **2008**, *24*, 5233–5237.

[87] Wu, X.; Ming, T.; Wang, X.; Wang, P. N.; Wang, J. F.; Chen, J. Y. High-photoluminescence-yield gold nanocubes: For cell imaging and photothermal therapy. *ACS Nano* **2010**, *4*, 113–120.

[88] Peng, Z. A.; Peng, X. G. Formation of high-quality CdTe, CdSe, and CdS nanocrystals using CdO as precursor. *J. Am. Chem. Soc.* **2001**, *123*, 183–184.

[89] Boldt, K.; Kirkwood, N.; Beane, G. A.; Mulvaney, P. Synthesis of highly luminescent and photo-stable, graded shell CdSe/$Cd_xZn_{1-x}S$ nanoparticles by *in situ* alloying. *Chem. Mater.* **2013**, *25*, 4731–4738.

[90] Jasieniak, J.; Smith, L.; van Embden, J.; Mulvaney, P.; Califano, M. Re-examination of the size-dependent absorption properties of CdSe quantum dots. *J. Phys. Chem. C* **2009**, *113*, 19468–19474.